applied sciences

MDPI

Article

Radiofrequency Performance Analysis of Metal-Insulator-Graphene Diodes

Leslie Paulina Cruz-Rodríguez [1], Mari Carmen Pardo [2], Anibal Pacheco-Sanchez [2], Eloy Ramírez-García [1], Francisco G. Ruiz [2] and Francisco Pasadas [2,*]

[1] Departamento de Telecomunicaciones, ESIME Zacatenco, Instituto Politécnico Nacional, Unidad Profesional Adolfo López Mateos, Avenida Instituto Politécnico Nacional s/n, UPALM, Edif. Z-4 3er Piso, Mexico City 07738, Mexico; lcruzr1400@alumno.ipn.mx (L.P.C.-R.); ramirezg@ipn.mx (E.R.-G.)

[2] Pervasive Electronics Advanced Research Laboratory (PEARL), Departamento de Electrónica y Tecnología de Computadores, Facultad de Ciencias, Universidad de Granada, 18071 Granada, Spain; mcpardo@ugr.es (M.C.P.); a.pacheco@ugr.es (A.P.-S.); franruiz@ugr.es (F.G.R.)

* Correspondence: fpasadas@ugr.es

Abstract: This work presents the performance projection of a metal-insulator-graphene diode as the building block of a radiofrequency power detector, highlighting its rectifying figures of merit. The analysis was performed by means of a computer-aided design tool validated with experimental measurements of fabricated devices. Transient simulations were used to accurately determine the detector output voltage, while particular consideration was given to suitable convergence of the non-linear circuit response. The diode was analyzed in both ideal and non-ideal cases, with the latter accounting for its parasitic effects. In the non-ideal case, the diode exhibited a tangential responsivity of 26.9 V/W at 2.45 GHz and 31.9 V/W at 1.225 GHz. However, when parasitic elements were neglected in the ideal case, the responsivity significantly increased to 47.3 V/W at 2.45 GHz and 38.7 V/W at 1.225 GHz. Additionally, the diode demonstrated a non-linearity of 6.64 at 0.7 V and an asymmetry of 806.6 in a bias window of ±1 V, which resulted in a competitive value compared to other state-of-the-art rectifying technologies. Tangential responsivities (β_v) of graphene diodes at less-studied frequencies in the gigahertz band are presented, showing a high β_v value of 63.7 V/W at 1 GHz.

Keywords: graphene; diode; radiofrequency; power detection; MIG

Academic Editor: Marco Rossi

Received: 31 March 2025
Revised: 14 May 2025
Accepted: 21 May 2025
Published: 24 May 2025

Citation: Cruz-Rodríguez, L.P.; Pardo, M.C.; Pacheco-Sanchez, A.; Ramírez-García, E.; Ruiz, F.G.; Pasadas, F. Radiofrequency Performance Analysis of Metal-Insulator-Graphene Diodes. *Appl. Sci.* **2025**, *15*, 5926. https://doi.org/10.3390/app15115926

1. Introduction

Graphene is a two-dimensional (2D) gapless material with outstanding transport properties, such as a high-carrier mobility and low surface resistance [1]. Graphene-based devices are suitable for high-frequency electronics applications with relaxed dimensions, such as amplifiers, power detectors, frequency multipliers, mixers, and phase shifters, among other circuits [1–3].

Metal-Insulator-Graphene (MIG) diodes are characterized by a bias-induced barrier height modulation at the graphene–metal interface, which dominates their performance [4]. Compared to conventional Metal-Insulator-Metal (MIM) diodes, the current–voltage (I-V) curve of MIG diodes presents enhanced zero-bias nonlinearity and responsivity, mainly due to the physical phenomena at the graphene–insulator interface [4].

An additional advantage of MIG diodes over their conventional counterparts is their versatility for fabrication on various substrates, including kapton [5], silicon, polyamide [6], and quartz [7]. This flexibility, combined with their high-current-driven capability [5] and

low junction capacitance [6], makes them attractive for high-frequency applications, such as radiofrequency (RF) power detection.

RF power detectors are essential blocks for collecting and measuring the electromagnetic energy of RF signals in applications such as RF identification (RFID), wireless communication, and energy harvesting [8]. To achieve optimal performance in these applications, power detectors are characterized by performance metrics such as operating frequency, dynamic range, sensitivity, tangential responsivity, and DC power consumption [9]. Precise power detectors have been demonstrated for both the square-law operation at low input power levels and the lineal regime at high powers [10]. Rectifying diodes have been widely employed to implement power detectors, showing, for example, a linear relationship between input power (P_{in}) and output voltage (V_{out}) at frequencies of 500 MHz up to a power level of −10 dBm [11], and a quadratic P_{in}–V_{out} response at power levels from 0 to 20 dBm for operating frequencies from 5 GHz to 6 GHz [12]. Regarding MIG diodes, dynamic ranges as high as 50 dB and tangential responsivities ranging from tens to a few hundreds of V/W have been reported around 2.4 GHz, whereas at 60 GHz, the rectifying capability decreases to 15 V/W [13,14]. Additionally, under DC conditions, voltage responsivities ranging from 10 V^{-1} up to a record 71 V^{-1} have been achieved [15].

In this work, performance projections of RF power detectors using MIG diodes based on a computer-aided design (CAD) tool calibrated with experimental measurements from fabricated devices are presented. The study is organized as follows: Section 2 presents the device and compact model calibration under static and dynamic conditions. Section 3 includes performance projection studies based on the model under different RF signals in a power detector. A discussion is included for each set of results. Section 4 draws the conclusions of this work.

2. MIG Device and Modeling

A physics-based model was calibrated with experimental data describing the static and dynamic performance of a MIG diode reported elsewhere [13]. The cross-section of the MIG diode used as a reference here and first reported in [4] is presented in Figure 1a. The fabrication process has been reported in detail in [4] and can be summarized as follows: The device consists of a Ti/Al alloy embedded metal electrode working as the anode, a TiO_2 dielectric grown by atomic layer deposition (ALD) with a thickness (t_{ox}) of 6 nm separating the top graphene layer from the anode and substrate, yielding an oxide capacitance per unit area $C_{ox} = \epsilon_{ox}\epsilon_0/t_{ox}$, considering $\epsilon_{ox} = 9$. A Ni cathode (20 nm tick) is located at one end of the graphene layer. The graphene layer length (L) is 2 µm and its width (W) is 80 µm. The fabrication process was conducted using optical contact lithography on a high-resistivity Si substrate (≈5 kΩcm) with a 1 µm thermal SiO_2 layer. The embedded metal layers forming the anode (180 nm Al, 20 nm Ti) were deposited (by e-beam evaporation followed by lift-off) in 200 nm deep trenches etched into the SiO_2 layer (via reactive ion etching). The dielectric was then deposited with an oxygen plasma process and the required rails for contacting the anode were opened through the TiO_2 layer with Ar plasma and sealed with 20 nm Ni. The graphene layer grown by chemical vapor deposition on copper foil was transferred to the device structured using a PMMA support layer. Oxygen plasma was used for graphene patterning, and the cathode (20 nm Ni, 100 nm Al) was fabricated by sputtering deposition and lift-off. After the graphene had been transferred onto the substrate, a characterization was performed using Raman spectroscopy, which confirmed that the transferred material consisted of single-layer graphene. Additionally, the carrier mobility was estimated to be in the range of 2000–3000 cm^2/Vs using a four-probe measurement setup [4].

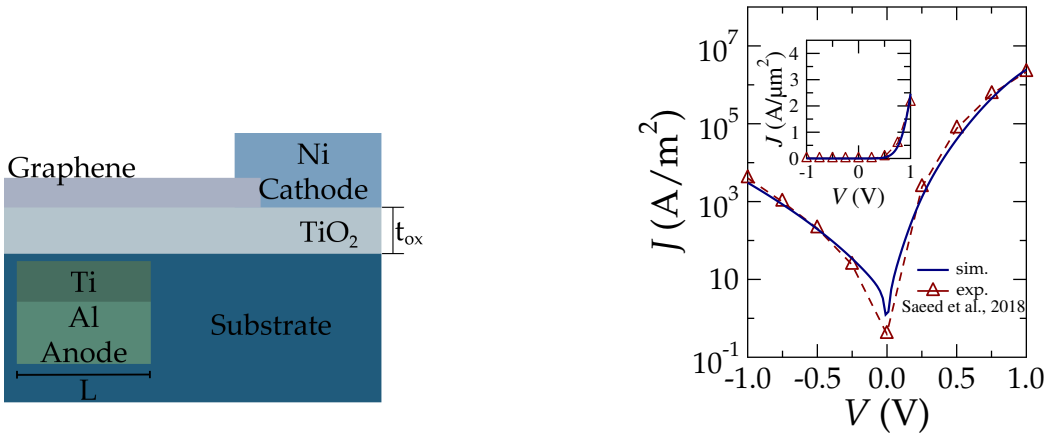

(**a**) (**b**)

Figure 1. (**a**) Device cross-section of the MIG diode under study and (**b**) current density versus applied voltage in a semilogarithmic scale. Markers are experimental data [13] and lines represent the modeling results. Inset shows the same plot in a linear scale.

The DC characteristics of the device were obtained by applying a voltage between −1 V and 1 V (cf. Figure 1b), whereas the RF power detection was characterized by using an RF power source at a selected operation frequency (f) under zero-bias conditions [13].

The large-signal compact model describing the thermionic transport within the MIG diode is based on the Dirac-Schottky model and includes image force lowering effects at the potential barrier. For the electrostatics, it considers the charge conservation principle and includes quantum capacitance and interface effects. Further technical details and specific model formulation are discussed in [16]. The resulting current density–voltage curve at a temperature of 295 K, showing the transition from reverse bias to forward bias, is presented in Figure 1b. A good agreement was achieved between the model and experimental results for both negative and positive biases.

The large-signal equivalent circuit of the MIG diode, including the extrinsic elements representing the parasitics due to metallic pads and dielectric surroundings, is presented in Figure 2 [16]. The dynamic phenomena of the internal graphene charge are described by the bias-dependent C_{int}. On the other hand, the transport is governed by the effects of the barrier formed at the graphene–insulator interface, modeled through a two-dimensional (2D) modified Dirac–Schottky equation [17], represented as the density current source J_{th} (current/device area). The extrinsic elements were extracted by applying a de-embedding procedure [18]. $C_{\mathrm{pa/pc}}$ represent the anode/cathode parasitic capacitance, both due to the substrate. $C_{\mathrm{f/fp}}$ is the parasitic diode fringe/pad capacitance, and $R_{\mathrm{a/c}}$ and $L_{\mathrm{a/c}}$ are the parasitic resistances and inductances associated with the anode and cathode pads, respectively [16].

The phenomena occurring at the interface between the graphene layer and the cathode contact are represented by the contact resistance R_{contact}. Nickel–graphene interfaces have been reported as Ohmic-like, with low values of contact resistances [19] (as expected for cathodes), and were used for the development of the selected technology, as well as other MIG-diode applications [13–15,20]. The value of 150 Ω for this device was achieved by considering R_{contact} as a fitting parameter [16]. The corresponding contact resistivity of 12 kΩ × μm of the graphene–Ni contact was larger than the one reported for these interfaces obtained with methods based on test structures [21]. This difference might be explained by a different fabrication process, yielding both a higher value of residual charge in the graphene used in the diode and a different contact geometry (top contact in [21], semi-embedded contact here).

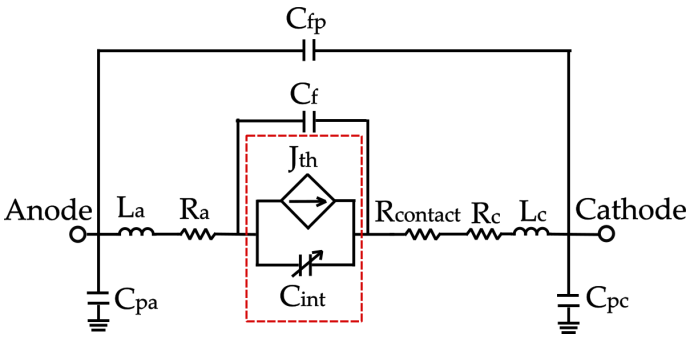

Figure 2. Large-signal equivalent circuit of the MIG diode [16]. Intrinsic elements are within the dashed box. The extrinsic (outside the dashed box) component values are $C_{fp} = 0.1$ fF, $C_f = 7.3$ fF, $C_{pa} = C_{pc} = 5.5$ fF, $L_a = L_c = 13$ pH, $R_a = R_c = 4.7\,\Omega$, and $R_{contact} = 150\,\Omega$.

An analysis of the simulated S-parameters (scattering parameters) of the diode including extrinsic elements (cf. Figure 2) was conducted over a frequency range of 100 MHz to 4 GHz. Figure 3a shows the magnitude of the reflection S-parameters S_{11} and S_{22} for bias voltages of −0.5 V, 0 V, and 0.5 V. As depicted, $|S_{11}|$ exhibited an identical response for the three different applied voltages; the impedance matching was poor, and thus most of the energy incident on the diode was reflected. The transmission parameters in Figure 3b consequently indicated a low transmission across the entire frequency range. In addition, reciprocal network conditions were found, i.e., $S_{12} = S_{21}$. Due to the reactance of the diode, the phase change of the S_{12} and S_{21} parameters was <120° in the frequency range under study, while the phase change of S_{11} and S_{22} was <90°. Further device engineering would be required to obtain specific phase shifts by adjusting the reactive elements in the diode (cf. Figure 2).

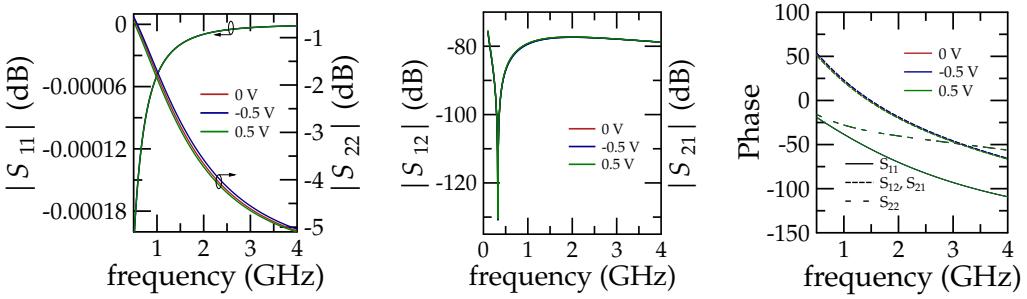

Figure 3. Scattering parameters. Magnitude in dB: (**a**) S_{11} and S_{22}, (**b**) S_{12} and S_{21}, (**c**) Phase of the scattering parameters.

3. Model-Based Performance Projection of MIG Rectifiers

3.1. Rectifying Metrics from DC Characteristics

To evaluate the performance characteristics of the MIG diode, three key figures of merit (FoMs) were considered: the DC responsivity f_{RES}, the nonlinearity f_{NL}, and the asymmetry factor f_{ASYM}. As for f_{RES}, it was defined as the ratio of the second derivative of the current with respect to the differential conductance, as shown in Equation (1). This FoM provided a first approximation of the output current increase with respect to the input power under square-law operation [22].

$$f_{RES} = \frac{1}{2} \cdot \frac{d^2 I}{dV^2} \left(\frac{dI}{dV} \right)^{-1} \tag{1}$$

Moving on to f_{NL}, this accounted for the diode nonlinearity and is expressed as the ratio of the differential conductance with respect to the conductance, as described in Equation (2),

$$f_{NL} = \frac{dI}{dV}\left(\frac{I}{V}\right)^{-1} \tag{2}$$

which represents the nonlinear response of the current with respect to the applied voltage.

Lastly, f_{ASYM} is defined as the absolute ratio of forward I_F to reverse I_R current, as shown in Equation (3), reflecting the balance between the positive and negative bias conditions.

$$f_{ASYM} = \left|\frac{I_F}{I_R}\right| \tag{3}$$

The resulting values of these FoMs as a function of bias are presented in Figure 4 for the MIG diode under study (cf. Figure 1), at room temperature (295 K) and with a voltage range between −1 V and 1 V. In Figure 4a, it can be observed that the highest responsivity value (14.65 V^{-1}) was achieved at 0 V, demonstrating that at this voltage, the diode was more sensitive to voltage changes and therefore suitable for zero-bias power detection. On the other hand, the nonlinearity showed an abrupt change near zero volts, as a consequence of the transition in bias. The highest nonlinearity value was reached under a large forward bias, i.e., 6.64 at 0.7 V. The asymmetry of the diode, depicted in Figure 4b, points to a significantly higher conduction under forward bias compared to reverse bias, as a result of the different injection mechanisms between the graphene and anode contact, with a value of 806.6 at 1 V.

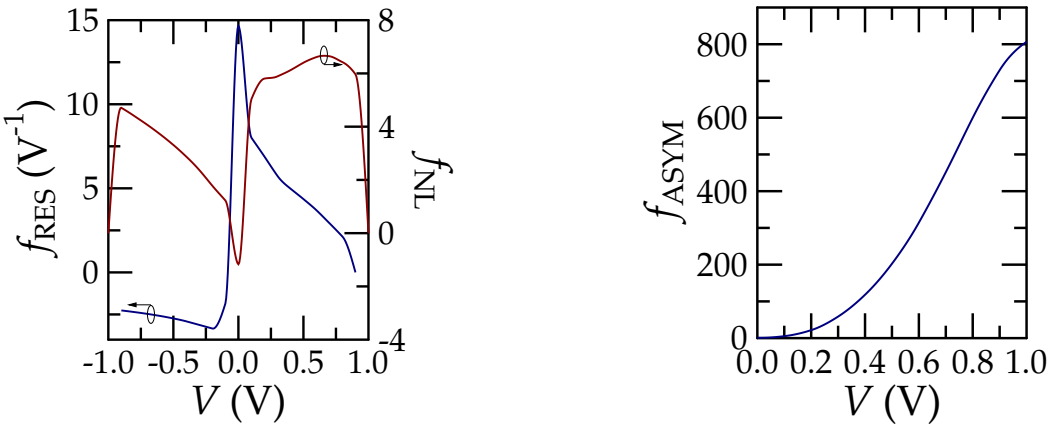

Figure 4. Figures of merit of the MIG diode under study: (**a**) responsivity (blue) and nonlinearity (red), and (**b**) asymmetry versus voltage.

3.2. Power Detection

A power detector operating at 1.225 GHz and 2.45 GHz was simulated to evaluate the performance of the fabricated MIG diode at zero bias for different RF input powers. The power detector was implemented as described in [16], using a impedance matching network to ensure power transfer through the diode and minimize signal reflections due to impedance mismatch. In this work, the experimental setup used for power detection as reported in [13] and simulated in [16] was considered, and hence, the results at frequencies different from 2.45 GHz should be considered as guidelines for performance projections in non-optimal matching scenarios. The topology of the MIG-based power detector can be seen in Figure 5, where the stages that are part of the circuit are shown. The power detector circuit included a 10 MΩ resistor at the output, representing the multimeter connected

to the circuit's output, which evaluated the maximum voltage value resulting from the applied RF input power.

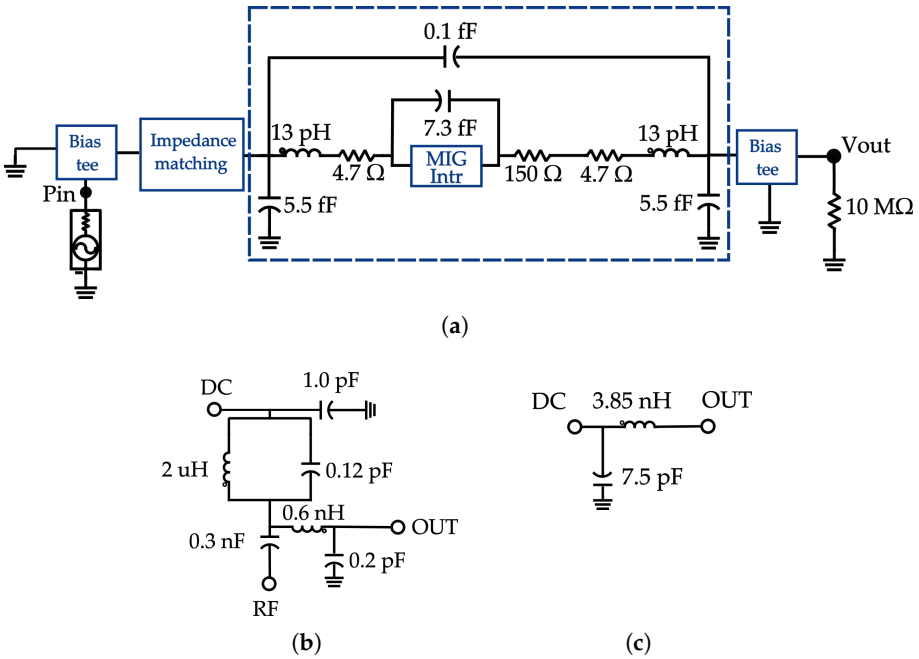

Figure 5. (**a**) Circuit used as a RF power detector (the dashed blue line encompasses the MIG large signal model including extrinsic elements); (**b**) bias tee, and (**c**) impedance matching network.

To evaluate the output voltage V_{out} of the power detector, a transient simulation was performed at each input power P_{in} for a given frequency. As an example, Figure 6a shows the transient response of V_{out} to an 10 dBm input signal, exhibiting that a steady-state was not achieved after 300 µs. To determine a single output voltage, convergence was sought by adding a reference voltage to the output of the circuit, to improve the initial condition used by the CAD tool [23]. This reference voltage should be as close as possible to either the expected result (provided measurements are known) or to a previously found solution for other power levels. By using a reference voltage, voltage convergence was achieved, as shown in Figure 6b. The lower P_{in}, the more cycles per second are required to be computed in order to achieve a steady-state solution.

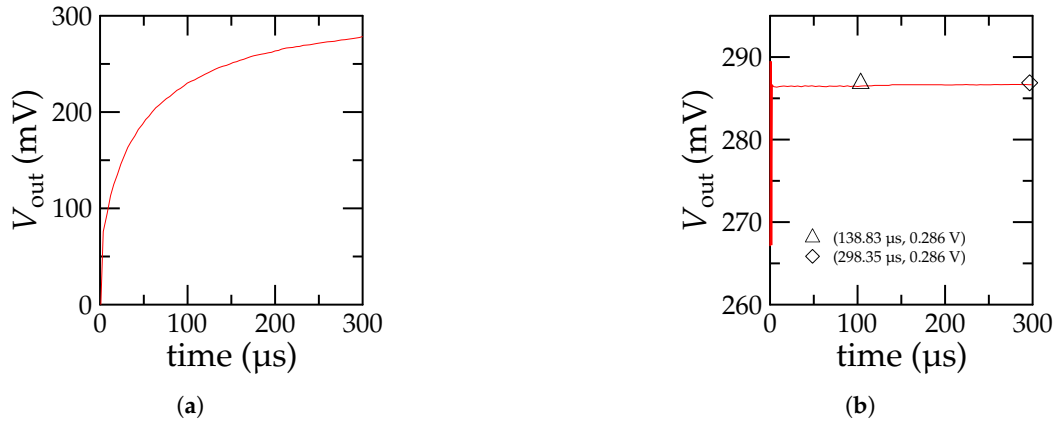

Figure 6. DC output voltage as a function of time for an input RF signal with a power of 10 dBm. (**a**) Transient response. (**b**) Steady-state response.

The power detector was simulated in transient analysis at different frequencies and input power levels ranging from −60 dBm to 20 dBm. Figure 7 shows its response, depicting

the variation in the output voltage V_{out} as a function of the input power P_{in}. Figure 7a shows the good agreement between the simulation results obtained here and experimental data at 2.45 GHz, specially in the range from −60 to 20 dBm. The measurement details have been presented elsewhere [13]. Since low-power level RF signals (i.e., below −40 dBm) are expected in various practical applications such as wireless communications systems or energy harvesters, it is important to properly describe the experimental data in such a range. In contrast to [16], where the simulation results deviated from the experimental data at low P_{in}, an accurate description of the measurements was obtained here by improving the convergence in the simulation framework, i.e., by increasing both the computational time and precision of the initial reference value for each transient simulation. The results for half the previous operating frequency, i.e., 1.225 GHz, showed lower V_{out} values at low P_{in}, whereas minimum differences were obtained at high P_{in}.

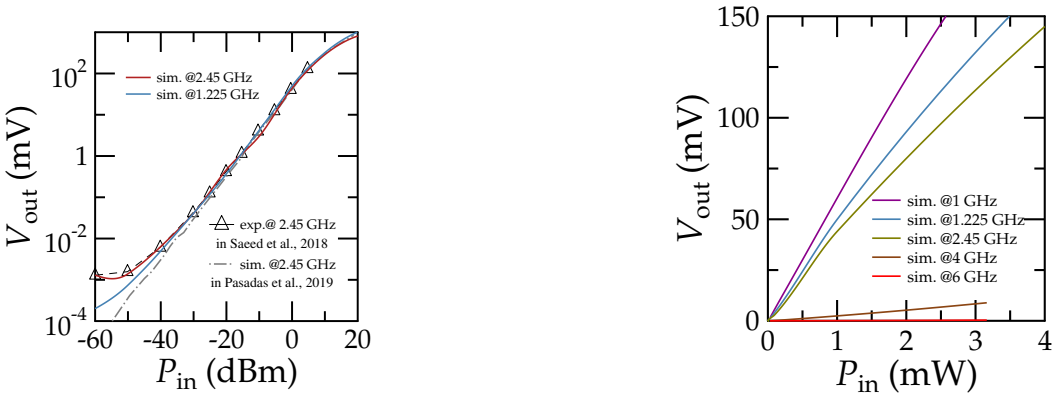

Figure 7. Output voltage versus input RF power at different frequencies. Plots in (**a**) semilogarithmic and (**b**) linear scale. Symbols represent experimental data [13], dashed lines are simulation results presented in [16], and solid lines are simulation results obtained in this work.

For high power levels, the RF tangential responsivity β_v of the power detector at the determined operation frequency was derived from the linear region of the output voltage as a function of the input power [24] as

$$\beta_v = \frac{V_{out}}{P_{in}} \tag{4}$$

To calculate the RF responsivity of the power detector, the power range from 0 mW to 4 mW was considered for several frequencies, as shown in Figure 7b. Figure 8 shows the tangential responsivity obtained in the range from 1 GHz to 6 GHz. The highest responsivity was achieved at the lowest evaluated value, i.e., 1 GHz, and then it followed a decreasing trend for higher frequencies. For frequencies above 4 GHz, β_v declined below 2.9 V/W, indicating the detector's reduced response capability beyond this frequency.

The MIG-based power detector was simulated at frequencies from 1 GHz to 8 GHz for powers of −15 dBm, −5 dBm, and 5 dBm, as shown in Figure 9. It can be observed that the power detector showed an almost linear response from 2 to 4 GHz. The detector indeed maintained a stable dynamic range up to 4 GHz, with an approximate increase by a factor of 10 in the output voltage for every 10 dB increase in input power. The change with frequency of V_{out} beyond this value was, however, power-dependent. While the highest and lowest power values considered followed very similar trends, an abrupt drop was observed for the −5 dBm curve at ∼5.5 GHz, in contrast to an apparent plateau appearing for the −15 dBm and 5 dBm curves. As a consequence, the results obtained here suggest

that between 7 GHz and 8 GHz, similar values of V_{out} were achieved for a 10 dB range of the input signal below −5 dBm.

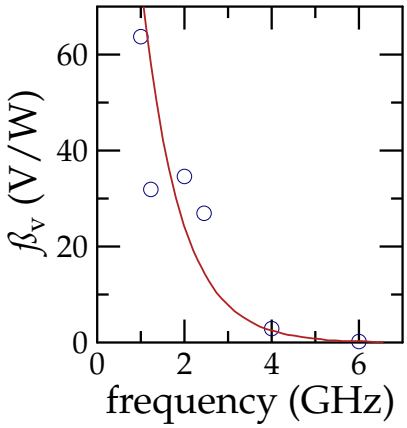

Figure 8. Variation in the device responsivity (markers) with frequency in the range from 1 GHz to 6 GHz. A line has been added as a guide for the eye to show the tendency, which follows an exponential fit.

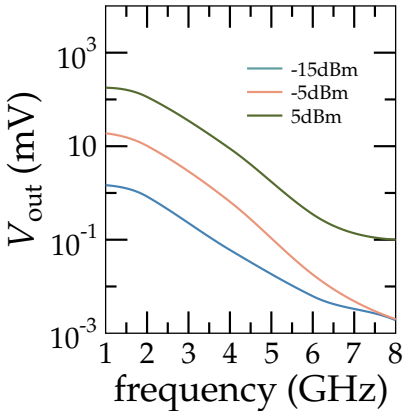

Figure 9. Output voltage versus frequency at different input RF power values.

To evaluate the ideal behavior of the power detector, the circuit in Figure 5 was simulated without considering the parasitic elements, and hence, only the intrinsic MIG diode was considered. The circuit was analyzed over an input power range of 0 to 20 dBm, as shown in Figure 10. The results indicate that, by removing the parasitic elements of the MIG diode, the detected output voltage increased, especially for the operation frequency at which the circuit was designed (i.e., 2.45 GHz). The RF tangential responsivities obtained without parasitic elements were 47.3 V/W and 38.7 V/W for 2.45 GHz and 1.225 GHz, respectively.

Table 1 presents a comparison of the FoMs from various works reporting the performance of fabricated MIG diodes, in both DC and RF modes, and the simulation results obtained here. The highest reported tangential responsivities are 168 V/W at 2.5 GHz [25] and 43.6 V/W at 2.45 GHz [16]. Notice that, in [25], the input power was not directly measured but evaluated from S_{11}, which might have led to an overestimation of β_v. As for DC, the highest recorded responsivity is 71 V^{-1} [15], while the nonlinearity reaches its maximum value of 11 at 0.7 V [4]. Finally, the technology addressed in this work showed a remarkable value for asymmetry of 806.6 at 1 V.

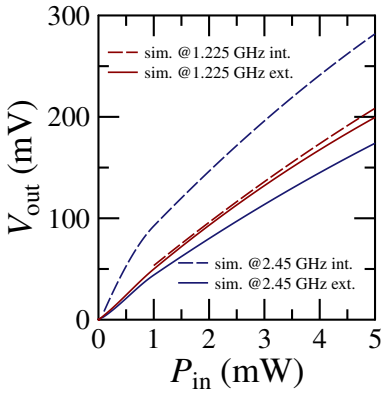

Figure 10. Output voltage versus input RF power at different frequencies with (dashed lines) and without (solid lines) parasitic elements.

Table 1. Comparison of figures of merit.

Ref.	f_{ASYM}	f_{NL}	* f_{RES}	β_v
this work	806.6 at 1 V	6.64 at 0.7 V	14.65 V^{-1}	63.7 V/W at 1 GHz, 31.9 V/W at 1.225 GHz, 34.6 V/W at 2 GHz, 26.9 V/W at 2.45 GHz, 2.9 V/W at 4 GHz and 0.2 V/W at 6 GHz
[4]	270 at 1.1 V	11 a 0.7 V	12 V^{-1} at 0.2 V	2.8 V/W at 2.4 GHz and 2.2 V/W at 30.8 GHz
[6]	18 at 0.9 V	3 at 0.3 V	8 V^{-1} at 0.1 V	-
[13]	-	-	-	42 V/W a 2.45 GHz
[20]	608	-	10 V^{-1}	-
[16]	-	-	12.4 V^{-1}	43.6 V/W at 2.45 GHz
[15]	-	-	71 V^{-1}	-
[25]	Up to 525	Up to 10	Up to 13.5 V^{-1}	15 V/W at 60 GHz and 168 V/W at 2.5 GHz
[26,27]	above 400	above 20	-	-
[28]	-	-	** 10–20 µS/V	-

* The values were modified according to Equation (1). ** Calculated as d^2I/dV^2; not directly comparable with f_{RES}.

The asymmetry value obtained in this work for the MIG diode demonstrated in [13] is among the highest reported in the literature, reflecting the excellent rectification ability of the diode. Additionally, the nonlinearity value is among the highest documented, highlighting the device's efficiency in applications such as harmonic generators, signal mixers, and frequency multipliers. The tangential responsivity achieved at 1 GHz also stands among the highest values reported in previous studies.

It is important to highlight that the input power range used to calculate the tangential responsivity varied among the different studies, which directly influenced the obtained values. For example, in [4], the input power range was from 0 mW to 3 mW, while in [25], a fixed power of −30 dBm was used. In [13,16], similar β_v values were reported at the same frequency, suggesting comparable input power ranges. In this work, a large range of 0 mW to 4 mW was employed, allowing for a more detailed evaluation of the detector's response. The tangential responsivity depends on the input power range, as the detector's behavior varies significantly across different operating regions. This explains why, even at similar frequencies, the reported values of β_v can range from tens to hundreds of V/W.

Furthermore, the impact of parasitics should be emphasized, as their removal led to a notable improvement in the β_v values. This optimization increased β_v by a factor of 1.75 times at 2.45 GHz and 1.21 times at 1.225 GHz, illustrating that reducing parasitic components is crucial for attaining higher tangential responsivity levels. This highlights

the need to further optimize the design of MIG diodes to reduce parasitic influences and improve performance.

4. Conclusions

A compact model of a metal-insulator-graphene diode calibrated with experimental measurements from fabricated devices was used to evaluate its rectifying figures of merit and project the performance of this device when used as an RF power detector under different conditions, such as various input power levels and operation frequencies. Transient simulations, supported by a reference voltage, enabled accurate evaluation of the output voltage, particularly at low levels of input power. The RF tangential responsivity of the power detector was found to exponentially decrease with frequency. In addition, a quasi-linear relationship between frequency and output voltage was obtained for frequencies between 4 GHz and 6 GHz. This relationship changed when considering the input power; at -15 dBm, the relationship showed no abrupt changes, whereas at 5.5 GHz, an abrupt drop was observed at -5 dBm, and an apparent plateau in the response was observed at 5 dBm. On the other hand, when analyzing the tangential responsivity of the detector without considering the diode's parasitic elements, a significant improvement in its performance was evident at 2.45 GHz, regardless of the input power; however, at lower frequencies, the difference between the ideal and non-ideal cases was only evident at input powers higher than 10 dBm. Additionally, the diode demonstrated a high asymmetry value of 806.6 at 1 V, showing its rectification performance. The nonlinearity value of 6.64 at 0.7 V is comparable with documented results, emphasizing its potential for nonlinear applications such as frequency multipliers or mixers. The results of this work are intended as a guideline to select appropriate conditions for the optimal operation of a MIG diode as a RF power detector.

Author Contributions: Conceptualization, L.P.C.-R. and A.P.-S.; methodology, L.P.C.-R. and A.P.-S.; software, L.P.C.-R., A.P.-S. and F.P.; validation, L.P.C.-R., A.P.-S., and F.P.; formal analysis, L.P.C.-R., M.C.P., and A.P.-S.; investigation, L.P.C.-R., and M.C.P.; resources, L.P.C.-R., E.R.-G., F.G.R., and F.P.; data curation, L.P.C.-R.; writing—original draft preparation, L.P.C.-R., M.C.P., and A.P.-S.; writing—review and editing, L.P.C.-R., M.C.P., A.P.-S., E.R.-G., F.G.R., and F.P.; visualization, L.P.C.-R.; supervision, L.P.C.-R., A.P.-S., E.R.-G., and F.P.; project administration, E.R.-G., F.P.; funding acquisition, E.R.-G., F.P., and F.G.R. All authors have read and agreed to the published version of the manuscript.

Funding: This work is part of the research project CNS2023-143727 RECAMBIO funded by MICIU/AEI/10.13039/501100011033 and the European Union NextGenerationEU/PRTR. This work was also supported in part by Secretaría de Ciencia, Humanidades, Tecnología e Innovación (Secihti), Mexico through Scholarship No. 1265593; by Consejería de Universidad, Investigación e Innovación de la Junta de Andalucía through the research project P21_00149 ENERGHENE. M. C. Pardo acknowledges the FPU program from the Spanish Ministry of Science and Innovation (MCIN) with reference FPU21/04904. F. Pasadas acknowledges the funding from the R+D+i project A-ING-253-UGR23 AMBITIONS co-financed by Consejería de Universidad, Investigación e Innovación and the European Union under the FEDER Andalucía 2021–2027. This work received additional support from the Dirección de Relaciones Internacionales and the Comisión de Operación y Fomento de Actividades Académicas del Instituto Politécnico Nacional and by Secretaría de Investigación y Posgrado under the contract SIP/20250027.

Institutional Review Board Statement: Not applicable.

Informed Consent Statement: Not applicable.

Data Availability Statement: The data from this study are available from the authors upon request.

Conflicts of Interest: The authors declare no conflicts of interest.

References

1. Ghivela, G.C.; Sengupta, J. The Promise of Graphene: A Survey of Microwave Devices Based on Graphene. *IEEE Microwave Mag.* **2020**, *21*, 48–65. [CrossRef]
2. Saeed, M.; Palacios, P.; Wei, M.-D.; Baskent, E.; Fan, C.-Y.; Uzlu, B.; Wang, K.-T.; Hemmetter, A.; Wang, Z.; Neumaier, D.; et al. Graphene-based microwave circuits: A review. *Adv. Mater.* **2022**, *34*, 2108473. [CrossRef] [PubMed]
3. Pasadas, F.; Medina-Rull, A.; Ruiz, F.G.; Ramos-Silva, J.N.; Pacheco-Sanchez, A.; Pardo, M.C.; Toral-Lopez, A.; Godoy, A.; Ramírez-García, E.; Jiménez, D.; et al. Exploiting ambipolarity in graphene field-effect transistors for novel designs on high-frequency analog electronics. *Small* **2023**, *19*, 2303595. [CrossRef] [PubMed]
4. Shaygan, M.; Wang, Z.; Elsayed, M.S.; Otto, M.; Iannaccone, G.; Ghareeb, A.H.; Fiori, G.; Negra, R.; Neumaier, D. High performance metal–insulator–graphene diodes for radio frequency power detection application. *Nanoscale* **2017**, *9*, 11944–11950. [CrossRef] [PubMed]
5. Fan, C.-Y.; Wei, M.-D.; Saeed, M.; Hamed, A.; Negra, R.; Wang, Z.; Shaygan, M.; Neumaier, D. Large-signal metal–insulator–graphene diode model on a flexible substrate for microwave application. In Proceedings of the IEEE MTT-S International Conference on Numerical Electromagnetic and Multiphysics Modeling and Optimization (NEMO), Reykjavik, Iceland, 8–10 August 2018. [CrossRef]
6. Wang, Z.; Uzlu, B.; Shaygan, M.; Otto, M.; Ribeiro, M.; González Marín, E.; Iannaccone, G.; Fiori, G.; Elsayed, M.S.; Negra, R.; et al. Flexible one-dimensional metal–insulator–graphene diode. *ACS Appl. Electron. Mater.* **2019**, *1*, 945–950. [CrossRef]
7. Hamed, A.; Saeed, M.; Wang, Z.; Shaygan, M.; Neumaier, D.; Negra, R. Graphene-diode-based frequency conversion mixers for high-frequency applications. In Proceedings of the IEEE MTT-S International Microwave Workshop Series on Advanced Materials and Processes for RF and THz Applications (IMWS-AMP), Bochum, Germany, 16–18 July 2019. [CrossRef]
8. Semple, J.; Georgiadou, D.G.; Wyatt-Moon, G.; Gelinck, G.; Anthopoulos, T.D. Flexible diodes for radio frequency (RF) electronics: A materials perspective. *Semicond. Sci. Technol.* **2017**, *32*, 123002. [CrossRef]
9. Ravanne, J.G.; Then, Y.L.; Su, H.T.; Hijazin, I. Microwave power detectors in different CMOS design architectures: A review. *IEEE Microw. Mag.* **2022**, *23*, 76–84. [CrossRef]
10. Zhang, T.; Eisenstadt, W.R.; Fox, R.M. A novel 5 GHz RF power detector. In Proceedings of the IEEE International Symposium on Circuits and Systems (ISCAS), Vancouver, BC, Canada, 23–26 May 2004. [CrossRef]
11. Milanovic, V.; Gaitan, M.; Marshall, J.C.; Zaghloul, M.E. CMOS foundry implementation of Schottky diodes for RF detection. *IEEE Trans. Electron Devices* **1996**, *43*, 2210–2214. [CrossRef]
12. Jeon, W.; Firestone, T.M.; Rodgers, J.C.; Melngailis, J. Design and fabrication of Schottky diode, on-chip RF power detector. *Solid-State Electron.* **2004**, *48*, 2089–2093. [CrossRef]
13. Saeed, M.; Hamed, A.; Wang, Z.; Shaygan, M.; Neumaier, D.; Negra, R. Graphene integrated circuits: New prospects towards receiver realisation. *Nanoscale* **2018**, *10*, 93–99. [CrossRef] [PubMed]
14. Saeed, M.; Hamed, A.; Negra, R.; Shaygan, M.; Wang, Z.; Neumaier, D. Zero-bias, 50 dB dynamic range, V-band power detector based on CVD graphene-on-glass. In Proceedings of the IEEE MTT-S International Microwave Symposium (IMS), Honolulu, HI, USA, 4–9 June 2017. [CrossRef]
15. Saeed, M.; Palacios, P.; Wei, M.-D.; Baskent, E.; Fan, C.-Y.; Uzlu, B.; Wang, K.-T.; Hemmetter, A.; Wang, Z.; Neumaier, D.; et al. Compact V-Band MMIC Square-Law Power Detector with 70 dB Dynamic Range Exploiting State-of-the-Art Graphene Diodes. In Proceedings of the 2021 IEEE MTT-S International Microwave Symposium (IMS), Atlanta, GA, USA, 6–11 June 2021; IEEE: New York, NY, USA, 2021; pp. 888–891. [CrossRef]
16. Pasadas, F.; Saeed, M.; Hamed, A.; Wang, Z.; Negra, R.; Neumaier, D.; Jiménez, D. Large-signal model of the metal–insulator–graphene diode targeting RF applications. *IEEE Electron Device Lett.* **2019**, *40*, 1005–1008. [CrossRef]
17. Ang, Y.S.; Yang, H.Y.; Ang, L.K. Universal Scaling Laws in Schottky Heterostructures Based on Two-Dimensional Materials. *Phys. Rev. Lett.* **2018**, *121*, 056802. [CrossRef] [PubMed]
18. Crupi, G.; Schreurs, D. (Eds.) *Microwave De-Embedding: From Theory to Applications*; Elsevier Science: Amsterdam, The Netherlands, 2013; ISBN 978-0-12-401700-9.
19. Shaygan, M.; Otto, M.; Sagade, A.A.; Chavarin, C.A.; Bacher, G.; Mertin, W.; Neumaier, D. Low Resistive Edge Contacts to CVD-Grown Graphene Using a CMOS Compatible Metal. *Ann. Phys.* **2017**, *529*, 1600410. [CrossRef]
20. Saeed, M.; Hamed, A.; Wang, Z.; Shaygan, M.; Neumaier, D.; Negra, R. Metal–insulator–graphene diode mixer based on CVD graphene-on-glass. *IEEE Electron Device Lett.* **2018**, *39*, 1104–1107. [CrossRef]
21. Gahoi, A.; Kataria, S.; Driussi, F.; Venica, S.; Pandey, H.; Esseni, D.; Selmi, L.; Lemme, M.C. Dependable Contact Related Parameter Extraction in Graphene–Metal Junctions. *Adv. Electron. Mater.* **2020**, *6*, 2000386. [CrossRef]
22. Cowley, A.M.; Sorensen, H.O. Quantitative comparison of solid-state microwave detectors. *IEEE Trans. Microw. Theory Tech.* **1966**, *14*, 588–602. [CrossRef]
23. Agilent Technologies. Transient and Convolution Simulation. September 2011. Available online: https://edadownload.software.keysight.com/eedl/ads/2011/pdf/cktsimtrans.pdf (accessed on 15 April 2025).

24. Qayyum, S.; Negra, R. Analysis and Design of Distributed Power Detectors. *IEEE Trans. Microw. Theory Tech.* **2018**, *66*, 4191–4203. [CrossRef]
25. Saeed, M.; Hamed, A.; Wang, Z.; Shaygan, M.; Neumaier, D.; Negra, R. Zero-Bias 50-dB Dynamic Range Linear-in-dB V-Band Power Detector Based on CVD Graphene Diode on Glass. *IEEE Trans. Microw. Theory Tech.* **2018**, *66*, 2018–2024. [CrossRef]
26. Baskent, E.; Wang, Z.; Lemme, M.C.; Negra, R. K-Band Graphene-Based Electrically Tunable Hybrid Coupler. In Proceedings of the 2024 IEEE Asia-Pacific Microwave Conference (APMC), Bali, Indonesia, 17–20 November 2024; pp. 1281–1283. [CrossRef]
27. Baskent, E.; Wang, Z.; Lemme, M.C.; Negra, R. Ka-Band Metal-Insulator-Graphene Diode-Based Thin-Film Cascaded Reflective-Type Phase Shifter. In Proceedings of the 2024 19th European Microwave Integrated Circuits Conference (EuMIC), Paris, France, 23–24 September 2024; pp. 311–314. [CrossRef]
28. Kunc, J.; Fridrišek, T.; Shestopalov, M.; Jo, J.; Park, K. Graphene–insulator–metal diodes: Enhanced dielectric strength of the Al_2O_3 barrier. *AIP Adv.* **2024**, *14*, 095207. [CrossRef]